

The mid-infrared colour-magnitude relation of early-type galaxies in the Coma cluster as measured by Spitzer-IRS*

M.S. Clemens¹, A. Bressan^{1,2,3}, P. Panuzzo⁴, R. Rampazzo¹, L. Silva⁵,
L. Buson¹, G.L. Granato⁵

¹INAF-Osservatorio Astronomico di Padova, Vicolo dell'Osservatorio, 5, 35122 Padova, Italy.

²SISSA-ISAS, International School for Advanced Studies, via Beirut 4, 34014 Trieste, Italy

³INAOE, Luis Enrique Erro 1, 72840, Tonantzintla, Puebla, Mexico

⁴Laboratoire AIM, CEA/DSM - CNRS - Université Paris Diderot, DAPNIA/Service d'Astrophysique, Bât. 709, CEA-Saclay, F-91191 Gif-sur-Yvette Cédex, France

⁵INAF, Osservatorio Astronomico di Trieste, Via Tiepolo 11, I-34131 Trieste, Italy

Accepted ?????. Received ????; in original form ?????

ABSTRACT

We use 16 μm , Spitzer-IRS, blue pickup photometry of 50 early-type galaxies in the Coma cluster to define the mid-infrared colour-magnitude relation. We compare with recent simple stellar population models that include the mid-infrared emission from the extended, dusty envelopes of evolved stars. The K_s -[16] colour in these models is very sensitive to the relative population of dusty AGB stars. We find that the *passively evolving* early-type galaxies define a sequence of approximately constant age (~ 10 Gyr) with varying metallicity. Several galaxies that lie on the optical/near-infrared colour-magnitude relation do not lie on the mid-infrared relation. This illustrates the sensitivity of the K_s -[16] colour to age. The fact that a colour-magnitude relation is seen in the mid-infrared underlines the extremely passive nature of the majority (68 %) of early-type galaxies in the Coma cluster. The corollary of this is that 32% of the early-type galaxies in our sample are *not* ‘passive’, insofar as they are either significantly younger than 10 Gyr or they have had some rejuvenation episode within the last few Gyr.

We also conclude that external effects, such as disruption of the dusty AGB star envelopes by the interstellar medium, does not effect the 16 μm emission. This mid-infrared emission is relatively short-lived and occurs well within the radius at which such effects become important. Given the robustness of mid-infrared emitting envelopes to environmental effects, the observation that galaxies with excess 16 μm emission lie preferentially at small radii within the cluster, indicates that the cluster environment influences the star formation history.

Key words: galaxies:elliptical and lenticular cD, galaxies:evolution, galaxies:clusters:general, galaxies:photometry.

1 INTRODUCTION

Early-type galaxies (ellipticals and S0s, ETGs hereafter) are ancient stellar populations whose epoch of formation is related to the large-scale structure formation in the Universe. This picture is supported by various studies that have used optical line-strength indices to determine evolutionary parameters of ETGs in the cluster and field environments (see Renzini 2006 for a review). Among these studies, some au-

thors (Bernardi et al. 2005, Clemens et al. 2006, Thomas et al. 2005, Sánchez-Blázquez et al. 2006a, Annibali et al. 2007) suggest that cluster ETGs have a luminosity weighted, mean stellar age 1-2 Gyr older than those in the field. Recently, Trager, Faber & Dressler (2008) challenged this view. Analyzing the Coma cluster, they found that the 12 ETGs in their sample have mean single stellar population equivalent ages of 5-8 Gyr, with the oldest systems being ≤ 10 Gyr old. This average age is remarkably similar to the mean age of ETGs in low density environments (see e.g. Annibali et al. 2007 and references therein).

The emission from elliptical galaxies longward of $\sim 10 \mu\text{m}$ has a large contribution from the circumstellar dust

* This work is based on observations made with the Spitzer Space Telescope, which is operated by the JPL, Caltech under a contract with NASA.

around evolved stars, such as those on the AGB. This dust emission has been detected by Spitzer in early-type galaxies where it is seen as a wide emission feature near $10\ \mu\text{m}$ with another broad feature near $18\ \mu\text{m}$ (Bressan et al., 2006). The spatial profile in the mid-infrared is similar to the optical profile (Temi et al., 2008, Athey et al. 2002), re-enforcing the notion that the origin is stellar rather than ISM. This circum-stellar dust has also been detected directly as an extended envelope around nearby AGB stars (Gledhill & Yates, 2003). Longer wavelength infrared emission from elliptical galaxies is sometimes detected (Leeuw et al., 2004; Marleau et al., 2006; Temi, Brighenti & Mathews, 2007.), but this cooler component is probably associated with a diffuse interstellar medium, rather than with evolved stars directly.

For objects older than 0.1 Gyr the mid-infrared emission traces stars during their mass-losing AGB phase, and this evolutionary phase is still detected in objects with ages typical of globular clusters such as 47 Tucanae (Lebzelter et al., 2006). Because the luminosity of an AGB star depends on its mass and the main sequence turn-off mass decreases with time, the mid-infrared emission depends on the age of the stellar population. If all the stars in an early-type galaxy were created in an instantaneous burst 10 Gyr ago, the mid-infrared emission would be dominated by stars on the AGB with an initial mass of slightly less than $1\ M_{\odot}$ (for solar metallicity).

The strength of the silicate emission from the dusty envelopes of evolved stars is a function of both age and metallicity. As pointed out by Bressan, Granato & Silva (1998) however, the dependence of this emission on age and metallicity is different to that in the optical.

A colour-magnitude relation which includes a band containing the silicate emission from AGB stars therefore traces the AGB population as a function of the total luminosity, and can, in principle, be used with the optical relation to disentangle the effects of age and metallicity.

Here, we use $16\ \mu\text{m}$ images of 50 ETGs in the Coma cluster, made with the blue peakup detector of the IRS on Spitzer. We combine these with archival Spitzer IRAC images at $4.5\ \mu\text{m}$ and K-band images to construct the mid-infrared colour-magnitude relation. As objects at the distance of the Coma cluster were too faint for IRS spectroscopy we include 4 galaxies in the Virgo cluster for which we have IRS spectra. These 4 objects were selected to have spectra that show no evidence of activity, such as recent star formation or an AGN, and are intended as a ‘template’ for passive objects against which to compare the more distant objects of Coma.

The Coma cluster is both very rich and dynamically relaxed, and contains some of the the most massive galaxies in the local Universe. As such, it is an ideal place to study the star formation history of ETGs.

2 DATA ANALYSIS AND RESULTS

2.1 Mid-infrared photometry

The blue peakup images (see appendix) are background dominated, with source fluxes only a few percent above the background level. In addition, the background shows fluctuations on spatial scales of several pixels. This presents a serious problem in the consistent determination of integrated

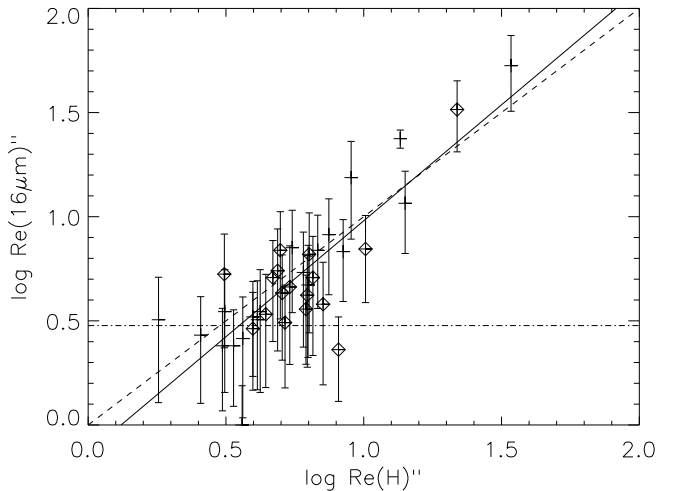


Figure 1. Relation between the effective H-band radii ($1.65\ \mu\text{m}$, Gavazzi et al. 2000) and the $16\ \mu\text{m}$ effective radii. The latter have been estimated by convolving a model $r^{1/4}$ de Vaucouleur’s law with the IRS blue peakup PSF (see text). Crosses are ellipticals and diamonds are lenticulars (classified either as S0/E, S0, SB0, or S0/a). The solid line is a least squares fit to the data whereas the dotted line corresponds to equal Re at both wavelengths. The horizontal dot-dashed line corresponds to the radius containing half of the encircled energy for the IRS blue peakup PSF.

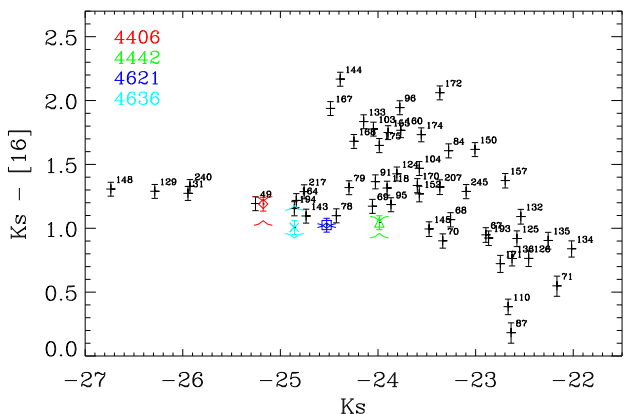


Figure 2. Mid-infrared colour-magnitude relation of the Coma cluster for fixed aperture K_s -[16] colours. Objects are identified according to their designations in Dressler (1980). The 4 ETGs in the Virgo cluster are shown with coloured symbols. For each of the Virgo galaxies the mid-infrared colours within the central $10''$ radius, as well as that of the whole galaxy *excluding* this central aperture are shown, as upward and downward pointing symbols, respectively. The assumed distance moduli to the Coma and Virgo clusters are 35.1 and 31.3 respectively.

fluxes for sources of different angular sizes. The standard technique of modeling the background as a smoothly varying light distribution, and then subtracting it from the image, tends to over-correct in the vicinity of larger sources, simply because the source size is similar to that of the background fluctuations. In order to avoid this problem we have opted to measure colours, rather than integrated fluxes, and to do so within a fixed angular radius of $12''$. The flux within this

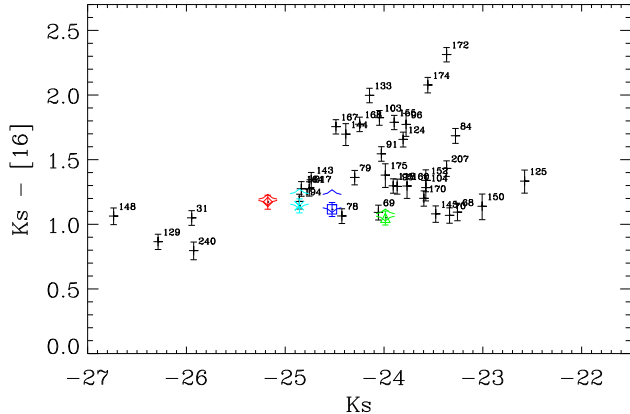


Figure 3. As fig. 2 but for photometry with circular radii equal to $2R_e$ where R_e is the effective radius of the galaxy measured in the H-band (Gavazzi et al., 2000). For the 4 Virgo galaxies a radius of only R_e was used due to the limited size of the pickup images.

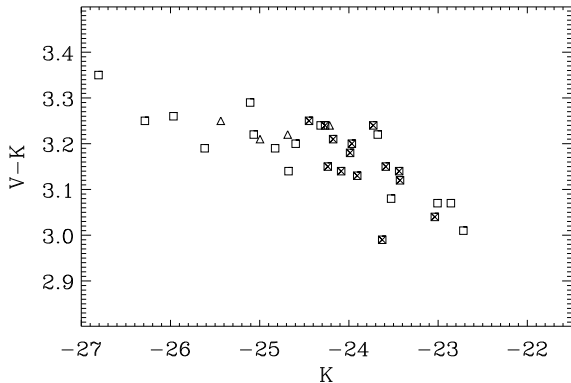


Figure 4. The optical/NIR colour-magnitude relation of the Coma cluster using the photometry of Bower, Lucey & Ellis (1992). Coma ETGs are shown as squares whereas the passive ETGs in the Virgo cluster are shown as triangles. Galaxies with a K_s -[16] excess are indicated with a cross.

radius is background corrected by subtracting the median pixel value within an annulus just outside this aperture. The error on the derived flux was taken as the quadrature sum of the rms variation within the annulus and the calibration error, which was taken as 5% for the blue pickup data.

Before applying the same procedure to IRAC channel 2¹ ($4.5 \mu\text{m}$) and 2MASS Ks-band ($2.2 \mu\text{m}$) images, these were convolved to the resolution of the IRS-pickup data, in order to remove colour gradients due to the differing instrumental resolutions. The measured aperture fluxes were then used to derive the colours for each object; these colours are presented in table 1.

Aperture photometry for the 4 Virgo elliptical galaxies was carried out in an analogous manner, but rather than use a circular aperture of radius $12''$, elliptical apertures of semi-major axis $72''$ were used. This difference takes account of

the fact that the Virgo cluster is 6 times closer than Coma cluster and that the images are well-resolved.

All aperture photometry was performed using a custom pipeline written in IDL and use was made of the *IDL Astronomy User's Library* (Landsman 1995).

2.2 Estimating the effective radii

A direct estimate of the effective radius based on an image with a high background level and fairly low signal-to-noise ratio would be rather sensitive to any error in the subtraction of the background level. In order to minimize this problem, rather than finding the radius containing half of the integrated flux, we adopted the following procedure. We first constructed a model galaxy with a de Vaucouleur's $r^{1/4}$ law and convolved it with the IRS blue pickup point spread function (PSF). We either assumed that the intrinsic ellipticity of each galaxy at $16 \mu\text{m}$ was the same as the optical value as given in “Goldmine”² or was circular, where no value was available. After convolution with the PSF we measured the radial profile in circular apertures and compared this to the same apertures measured on the image. The derived value of the effective radius, R_e , is that of the model galaxy whose PSF-convolved FWHM was equal to that of the image profile. These values are given in table 1 along with effective radii measured at $1.65 \mu\text{m}$ by Gavazzi et al. (2000). The error on the estimate of the effective radii was estimated using a Monte-Carlo approach. To the model galaxy, convolved with the IRS blue pickup PSF, Gaussian noise was added at the level present in the real images. For 200 realizations of this noise, the FWHM was measured using the same procedure as for the real images. The distribution of these values (as a function of S/N ratio) was used as an estimate of the error on the derived values of R_e .

A comparison between the H-band and $16 \mu\text{m}$ effective radii is shown in fig. 1. Clearly, most galaxies in Coma are barely resolved by Spitzer-IRS, however, for those that are clearly resolved their effective radii are similar to those in the near-infrared. There is no evidence, for example, that the $16 \mu\text{m}$ emission is derived from an unresolved central source. Similar effective radii in the near and mid-infrared are expected if the mid-infrared emission is stellar in origin, such as found by Temi et al. (2008).

2.3 The mid-infrared colour-magnitude diagram

In figure 2 we show the mid-infrared colour-magnitude diagram of the Coma cluster. The K_s -[16] colour is shown as measured within a fixed aperture of 12 arcsec.

The distribution of K_s -[16] colour shows a steady reddening from the faintest magnitudes observed ($K_s \sim -22$) to $K_s \sim -24$. In this magnitude range the dispersion in $K_s - [16]$ is close to a magnitude with values as high as 2.2 near $K_s \sim -24$. At brighter magnitudes the colours show little variation and low dispersion with $K_s - [16] \simeq 1.3$.

We also plot the position of four selected *passive* ETGs in the Virgo cluster, selected from the sample of Bressan et al. (2006). These galaxies have nuclear MIR spectra whose main characteristic is the presence of the silicate bump above

¹ Calibration errors taken as 10% , although the real calibration errors may be smaller.

² <http://goldmine.mib.infn.it/>, Gavazzi et al. (2003)

Source ID	GMP83	R.A. (J2000)	Dec. (J2000)	Type	Ks mag	4.5-16	K _s - 16	$R_e(H)$ "	$R_e(16\ \mu m)$ "
31	4928	12h57m24.35s	+27d29m51.8s	E/S0	9.20	—	1.27 ± 0.056	21.82	32.7 ± 12.2
49	1750	13h01m53.75s	+27d37m27.9s	E	—	—	1.19 ± 0.056	8.42	6.8 ± 2.9
67	3493	12h59m24.93s	+27d44m19.9s	S0	—	0.87 ± 0.118	0.95 ± 0.059	—	3.2 ± 1.9
68	3660	12h59m13.49s	+27d46m28.7s	S0	11.89	0.99 ± 0.117	1.07 ± 0.057	7.12	3.8 ± 2.2
69	3730	12h59m08.00s	+27d47m02.7s	E	11.09	1.19 ± 0.116	1.17 ± 0.056	6.28	4.7 ± 2.6
70	3739	12h59m07.51s	+27d46m04.1s	E	11.81	0.86 ± 0.117	0.90 ± 0.058	3.13	3.5 ± 2.1
71		12h58m57.50s	+27d47m07.5s	S0	12.98	0.43 ± 0.128	0.55 ± 0.082	—	2.3 ± 1.5
78	2000	13h01m31.70s	+27d50m50.2s	E	10.72	1.11 ± 0.116	1.10 ± 0.056	5.50	7.1 ± 3.6
79	2157	13h01m17.50s	+27d48m33.0s	S0	10.85	1.26 ± 0.116	1.32 ± 0.056	4.68	5.1 ± 2.6
84	2956	13h00m05.30s	+27d48m26.8s	S0	11.87	1.54 ± 0.117	1.61 ± 0.056	5.39	4.6 ± 2.7
87	3403	12h59m30.64s	+27d47m29.1s	E	12.51	0.16 ± 0.129	0.18 ± 0.083	—	1.7 ± 1.4
91	3997	12h58m48.50s	+27d48m37.3s	S0	11.12	1.29 ± 0.116	1.36 ± 0.056	5.06	4.3 ± 2.3
95		13h02m52.73s	+27d51m59.6s	S0	11.28	—	1.19 ± 0.056	4.41	3.4 ± 1.9
96		13h01m50.22s	+27d53m36.8s	E	11.37	1.82 ± 0.116	1.94 ± 0.056	3.62	1.0 ± 0.5
103	3400	12h59m30.60s	+27d53m03.2s	S0/a	11.10	1.73 ± 0.116	1.78 ± 0.056	3.96	2.9 ± 1.4
104	3296	12h59m37.90s	+27d54m26.1s	S0	11.57	1.37 ± 0.116	1.47 ± 0.056	3.12	5.3 ± 3.0
110	4626	12h57m50.62s	+27d52m45.8s	S0/E	12.48	0.39 ± 0.119	0.39 ± 0.062	—	2.3 ± 1.4
118	2541	13h00m39.50s	+27d55m26.5s	E	11.24	1.25 ± 0.116	1.32 ± 0.056	6.04	5.4 ± 3.0
124	3201	12h59m44.30s	+27d54m44.6s	E	11.34	1.40 ± 0.116	1.43 ± 0.056	4.11	3.2 ± 1.7
125	3222	12h59m42.31s	+27d55m29.1s	E	12.57	0.85 ± 0.120	0.92 ± 0.063	1.80	3.2 ± 1.9
126		12h59m44.00s	+27d57m30.3s	S0	12.69	0.71 ± 0.120	0.76 ± 0.064	—	5.5 ± 2.6
129	3329	12h59m35.71s	+27d57m33.8s	D	8.86	1.26 ± 0.116	1.29 ± 0.056	34.23	53.1 ± 21.0
132	3487	12h59m25.31s	+27d58m04.7s	S0	12.61	0.98 ± 0.118	1.09 ± 0.059	—	3.5 ± 2.1
133	3639	12h59m15.00s	+27d58m14.9s	E	11.00	1.87 ± 0.116	1.84 ± 0.056	3.37	2.4 ± 1.2
134		12h59m03.85s	+27d57m32.6s	E	13.13	0.92 ± 0.120	0.84 ± 0.065	—	2.2 ± 1.2
135	3851	12h58m59.86s	+27d58m02.6s	E	12.89	0.54 ± 0.122	0.90 ± 0.068	—	3.9 ± 1.8
136	3914	12h58m55.30s	+27d57m52.5s	E	12.52	0.73 ± 0.117	0.76 ± 0.059	—	2.0 ± 0.9
143	2390	13h00m54.46s	+28d00m27.3s	E	10.41	1.07 ± 0.116	1.10 ± 0.056	9.00	15.4 ± 7.6
144	2516	13h00m42.76s	+27d58m16.6s	S0/a	10.76	2.10 ± 0.116	2.17 ± 0.056	6.17	3.6 ± 1.6
145	2535	13h00m40.70s	+27d59m47.9s	S0	11.67	0.92 ± 0.118	0.99 ± 0.059	4.87	5.5 ± 3.2
148	2921	13h00m08.13s	+27d58m37.1s	D	8.41	1.28 ± 0.116	1.31 ± 0.056	13.57	23.7 ± 2.4
150	2940	13h00m06.20s	+28d00m14.7s	E	12.14	1.49 ± 0.116	1.62 ± 0.056	4.21	3.5 ± 2.1
152	3170	12h59m46.79s	+27d58m26.0s	SB0	11.57	1.18 ± 0.119	1.27 ± 0.063	6.34	6.6 ± 3.8
155	3367	12h59m32.82s	+27d59m01.2s	S0	11.25	1.66 ± 0.116	1.75 ± 0.056	5.18	3.1 ± 1.6
157	3484	12h59m25.46s	+27d58m23.7s	S0	12.45	1.26 ± 0.117	1.37 ± 0.058	—	10.9 ± 4.9
160	3761	12h59m05.90s	+27d59m48.2s	SB0	11.38	1.64 ± 0.117	1.77 ± 0.058	6.24	4.2 ± 2.3
164		13h03m00.89s	+28d01m57.2s	S0	10.31	—	1.22 ± 0.056	10.15	7.0 ± 3.1
167	2417	13h00m51.57s	+28d02m34.2s	S0/E	10.66	1.88 ± 0.116	1.94 ± 0.056	8.10	2.3 ± 1.0
168	2440	13h00m48.67s	+28d05m26.9s	E	10.90	1.58 ± 0.116	1.68 ± 0.056	3.96	3.3 ± 1.6
170	2727	13h00m22.00s	+28d02m50.1s	SB0	11.55	1.22 ± 0.117	1.34 ± 0.056	6.54	5.1 ± 2.9
171		13h00m16.90s	+28d03m50.0s	S0	12.40	0.74 ± 0.122	0.72 ± 0.069	—	3.6 ± 2.2
172	2839	13h00m14.60s	+28d02m28.6s	E	11.78	1.98 ± 0.116	2.06 ± 0.056	3.07	2.4 ± 1.2
174	2922	13h00m07.80s	+28d04m42.7s	E	11.59	1.66 ± 0.116	1.73 ± 0.056	2.56	2.7 ± 1.4
175	3073	12h59m55.90s	+28d02m04.9s	S0	11.16	1.52 ± 0.117	1.65 ± 0.057	4.98	6.9 ± 3.7
193	3084	12h59m55.10s	+28d07m42.2s	E	12.28	0.87 ± 0.117	0.92 ± 0.058	—	3.8 ± 2.3
194	3792	12h59m03.79s	+28d07m25.6s	E	10.29	1.13 ± 0.117	1.15 ± 0.057	6.81	6.9 ± 3.3
207	2912	13h00m09.14s	+28d10m13.6s	E	11.78	1.20 ± 0.118	1.32 ± 0.059	3.64	2.6 ± 1.5
217	3055	12h59m57.60s	+28d14m50.6s	E	10.39	1.23 ± 0.116	1.29 ± 0.056	7.47	8.2 ± 4.0
240	4822	12h57m31.95s	+28d28m37.0s	E	9.22	—	1.33 ± 0.056	14.13	11.6 ± 4.9
245		12h56m56.58s	+28d37m24.1s	S0	12.05	—	1.29 ± 0.057	—	3.2 ± 1.6

Table 1. The integrated 16 μm fluxes and sizes of the sample ETGs. The flux errors are the quadrature sum of a term due to the uncertainty in deriving the background sky level and a 5% calibration uncertainty. The effective radii have been calculated by convolving a model $r^{1/4}$ de Vaucouleur’s law with the IRS blue peakup PSF (see text).

10 μm , indicating a passively evolving stellar population. These galaxies have also been observed in the IRS Peakup mode to secure a link between photometric and spectroscopic observations.

The presence of stellar population gradients within ETGs (Annibali et al. 2007), together with the existence of a general increase of the effective radius with the total mag-

nitude of the galaxy, could, however, introduce a spurious effect, since a fixed aperture measurement would probe stellar populations in relatively more central regions for brighter galaxies.

To quantify this effect we repeated the measurement within a fixed *relative* aperture of radius $\sim 2 R_e$, where R_e is the effective radius of the galaxy. The results are shown

in fig. 3, though the lack of measured H-band effective radii introduces a cut at magnitudes fainter than $K_s \sim -23$. In this figure the flattening at magnitudes brighter than $K_s \sim -24$ becomes more evident and actually the slope of the colour-magnitude relation is reversed for the brightest Coma galaxies, while there are only small differences at magnitudes fainter than $K_s \sim -24$.

The position of the four passive Virgo galaxies in fig. 2 and that of the Coma galaxies brighter than $K_s \sim -24$ define a tight relation that can be extended down to the faintest magnitudes. By analogy with optical/NIR colour-magnitude relations and because of the presence of the four Virgo ETGs we argue that this line represents the MIR colour-magnitude relation of *passively evolving*, ETGs in the Coma cluster. ETGs significantly above this line have an “excess” of $16 \mu\text{m}$ emission with respect to the passive sequence.

The presence of a population of galaxies which appear anomalously red in the mid-infrared colour-magnitude diagram is not mirrored in the optical/near-infrared, fig. 4. The V-K colour shows a steady increase towards brighter magnitudes with a slight flattening for objects brighter than $K \sim -24$. This, in fact, is very similar to what we identify above as the *passive* colour magnitude relation in the mid-infrared. The implications of this difference are discussed further below.

3 DISCUSSION

From an extrapolation of the NIR stellar photospheric continuum into the mid-infrared Bressan et al. (2006) have estimated that the $16 \mu\text{m}$ emission in passive, ETGs has approximately equal contributions from stellar photospheres and dust emission. The most likely origin of the latter emission is from dusty circumstellar envelopes around evolved stars, such as the mass losing Asymptotic Giant Branch (AGB) stars. The exact proportions depend on parameters such as the age and metallicity of the stellar population. Because the photospheric contribution shows little variation for a fixed K-band magnitude, the mid-infrared colour-magnitude relation should depend strongly on the population of dusty AGB stars as a function of galaxy luminosity. In this scenario, those ETGs that show an excess of $16 \mu\text{m}$ emission have the largest luminosity-weighted dusty AGB population. The evolution of this stellar population should therefore be critical to the interpretation of the mid-infrared colour-magnitude diagram.

Another possible origin of an excess of emission at $16 \mu\text{m}$ could be the contribution of a central AGN, as seen in the spectrum of NGC 4486 (Bressan et al. 2006). However, there is no evidence of broad emission lines in the available SDSS spectra of those galaxies which lie well above the ‘passive’ colour-magnitude relation in fig. 2. There is also no evidence that these galaxies have smaller effective radii at $16 \mu\text{m}$ (as shown by NGC 4486, that appears unresolved in the SL and LL IRS apertures).

3.1 Influence of the inter-stellar environment

Before considering the colour-magnitude relation in terms of stellar evolution, we first consider the influences that the environment might have on the mid-infrared colours. In nearby

AGB stars a significant fraction of the $16 \mu\text{m}$ flux originates from extended, dusty, circumstellar envelopes. It is thus important to understand how robust these envelopes are to different external perturbations, such as the ram-pressure of the interstellar medium (ISM) in the central regions of massive ellipticals.

The circumstellar envelope of an AGB star expands at a typical velocity of $\sim 10 \text{ km s}^{-1}$ which, at the condensation radius ($R_c \sim 10^{14} \text{ cm}$), is of the order of the escape velocity. The MIR emission, $f(\nu)$, in AGB stars, has a broad maximum between 10 and $20 \mu\text{m}$ suggesting a dust temperature $T_{\text{dust}} \sim 300 \text{ K}$. Inspection of our dusty circumstellar models shows that dust reaches this temperature only in a thin internal region of the envelope, whose size is a few tens of R_c .

At 10 km s^{-1} the crossing time of this region is only 100 yr. Thus, the MIR emission from AGB stars is a short lived phenomenon: after about 100 yr, dust is already so cool that its contribution in the MIR spectral region becomes negligible.

However, in the central regions of an ETG, the star moves at the dispersion velocity through the tenuous ISM, and we need to determine whether or not the circumstellar envelope is able to maintain its structure in the inner few tens of R_c .

In order to estimate the radius at which the organized structure of the envelope is destroyed by its interaction with the ISM, we equate the kinetic energy density in the circumstellar wind ($\sim 1/2 \rho_C v_\infty^2$) to the kinetic energy density of the ISM, due to the stellar dispersion velocity, ($\sim 1/2 \rho_I \sigma_g^2$).

Using a stationary wind the circumstellar gas density is

$$\rho_C = \frac{\dot{M}}{4\pi r^2 v_\infty} \quad (1)$$

while the ISM density is evaluated from the mass that has been already lost by stars

$$\rho_I = \frac{d^2 M}{dt dM_*} \times t \times \rho_* \simeq 10^{-12} \times t \times \rho_* \quad (2)$$

In the second equation $d^2 M / dt dM_* \simeq 10^{-12} \text{ yr}^{-1}$ is the typical gas deposition rate per unit time and per unit stellar mass from the old stellar population. The average stellar density, ρ_* , is evaluated from deprojection of the De Vaucouleurs law (Young 1976) and depends on the assumed position within the galaxy.

Applying the condition of virial equilibrium and the observed relation between the total galaxy mass and the velocity dispersion (Cappellari et al. 2006) we find

$$r/r_c \simeq 200 \sqrt{\frac{\dot{M}_8 v_{10}}{L_3} \frac{1}{\sigma_3^{1.78} \rho_{01} t_{\text{Gyr}}}} \quad (3)$$

In this equation, r_c is the condensation radius, $\sim 1.66 \times 10^{12} \sqrt{L/L_\odot}$, for a silicate dust mixture (for graphite r_c is about half this value and r/r_c must be doubled); \dot{M}_8 is the stellar mass loss rate in $10^{-8} M_\odot/\text{yr}$; v_{10} is the wind velocity in units of 10 km s^{-1} ; L_3 is the luminosity in units of $10^3 L_\odot$; σ_3 is the stellar velocity dispersion in units of 300 km s^{-1} ; r_e is the effective radius of the galaxy; ρ_{01} is the dimensionless average stellar density with respect to its value at $r/r_e = 0.1$ ($\rho_{01} = 10.5$, Young, 1976); M_{12} is the galaxy mass in units of $10^{12} M_\odot$ and t_{Gyr} is the time in Gyr.

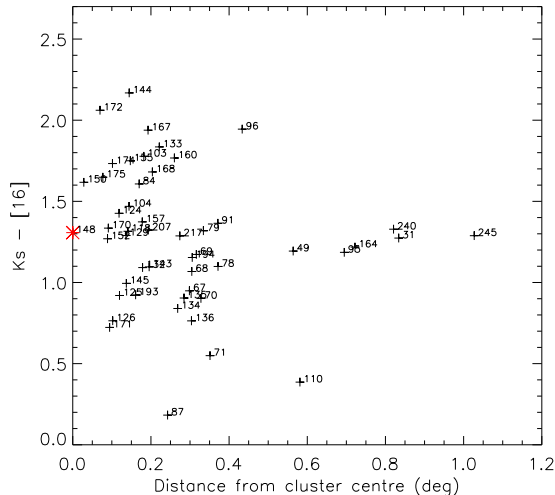


Figure 5. K_s -[16] colour plotted as a function of the projected distance from the cluster centre, defined as the CD galaxy D148 (asterisk on y-axis).

Thus, only for very low mass-loss rates ($10^{-10} M_{\odot}/\text{yr}$) or in the very central regions of a galaxy - $\rho(r/r_e = 0.01) = 357$ - may the structure of the wind be destroyed at a few condensation radii. We may thus conclude that, in all relevant cases, the circumstellar wind is not destroyed by its interaction with the environment even in the cores of ETGs.

Once the circumstellar envelope mixes with the ISM, dust grains may be destroyed via sputtering by the hot ($\sim 10^7$ K) ISM gas. This process, however, will not affect the MIR emission, because, as discussed above, when the dust is released to the ISM it is already too cool to emit in the MIR spectral region. Furthermore, the timescale for dust grain destruction via sputtering, even in the centre of the Coma cluster, is $\sim 10^8$ yr (Dwek, Rephaeli & Mather, 1990), much larger than the lifetime of the newly formed hot dust within the circumstellar envelope (~ 100 yr).

Finally we plot, in fig. 5, the K_s -[16] colour as a function of projected distance from the cluster centre. This figure shows that there is no particular trend with the cluster environment. We anticipate, however, that the galaxies showing a K_s -[16] colour excess seem more concentrated towards the cluster centre. We will return to this in the discussion.

In summary, we conclude that the MIR emission from dust grains in AGB stars is a short lived phenomenon (~ 100 yr) happening in the inner, denser region of the circumstellar envelopes. This emission cannot easily be modified by interaction with the environment, so that the environment does not have a *direct* influence on the mid-infrared colour-magnitude relation.

3.2 Stellar Evolution

As it appears that the form of the MIR colour-magnitude relation is not influenced directly by some particular environmental effect, it must be explained via the properties of the underlying stellar populations.

In Figure 6 we compare our observations with the pre-

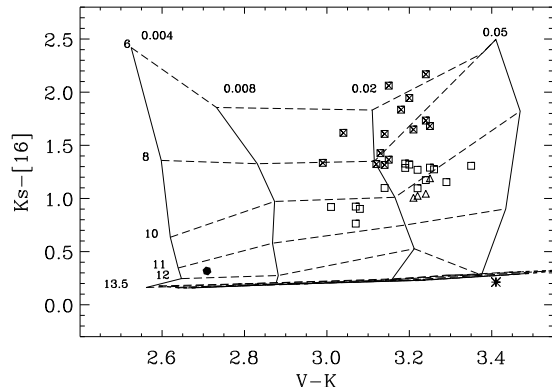


Figure 6. Optical NIR MIR colour-colour diagram. The horizontal axis is the V-K colour from the precision photometry of Bower, Lucey & Ellis (1992) while the vertical axis is the K_s -[16] colour. Squares are Coma ETGs and triangles are the four selected passive ETGs in the Virgo cluster. SSP models for the indicated ages and metallicity are computed following the scheme of Bressan et al. (1998). Models without dusty AGB envelopes collapse to the almost horizontal dashed lines at the bottom of the diagram. The dotted line represents the locus of the Kurucz model atmosphere with low metallicity (the effect of metallicity is very small however) and the asterisk is a COMARCS low temperature atmosphere model as calculated by Aringer et al. (2008, in prep.) The position of the globular cluster, 47-Tuc, is indicated by the solid hexagon in the lower left.

dictions for the integrated colours of simple stellar populations (SSPs).

As discussed in Bressan et al. (1998) both the integrated optical and MIR colours of SSPs suffer from the degeneracy between age and metallicity, but in the opposite sense. While optical features (colours or narrow band indices) of the same strength can be obtained by an *anti-correlated* variation of age and metallicity, producing the typical banana-shaped solutions in the age-metallicity diagrams (Annibali et al. 2007), an equal intensity of the $10\mu\text{m}$ bump may be obtained by a *correlated* variation of the age and metallicity.

For this reason, the effects of age and metallicity variations are best separated in a mixed optical-NIR-MIR colour-colour plot, such as that in Fig. 6.

In Fig. 6 the horizontal axis is the V-K colour obtained from the precision photometry of Bower, Lucey & Ellis (1992), while the vertical axis is our measured K_s -[16] colour. Though the V-K colours of Bower, Lucey & Ellis are provided only for a sub-sample of our galaxies (30 out of 50 objects), we prefer to use their values to preserve the homogeneity of the data. Squares are the Coma ETGs while the triangles refer to the four Virgo galaxies.

New SSP models, for the indicated age and metallicity, have been computed following the scheme of Bressan et al. (1998). The only difference with respect to these previous models is a minor revision of the mass loss rate during the AGB phase, introduced by the calibration with new V-K integrated colours of populous star clusters in the Large Magellanic Cloud, and the adoption of the new empirical library of stellar spectra (Sánchez-Blázquez et al., 2006b).

A few caveats concerning models should be kept in mind because they are relevant to the present investigation.

First of all, it is worth recalling that in Bressan et al.

(1998) the effects of possible circumstellar dust in the red giant branch (RGB) phase (i.e. before central helium burning in the horizontal branch in the case of old populations) have not been considered. Recent claims, that RGB stars also show a significant MIR excess not dependent on their luminosity (Origlia et al. 2007), should be regarded with great care because of possible strong crowding effects (Boyer et al. 2008).

Furthermore, old stellar populations in the galaxies we are considering could reach super-solar metallicity and, as such, may not be well represented by those in our own galaxy. Very little is actually known on the efficiency of the mass-loss rate at high metallicity (Carraro et al. 1996). However, van Loon et al. (2008) do not find evidence of a MIR excess in the RGB stars of NGC 6791, a super metal-rich globular cluster. Also, NGC 4649 and NGC 1399, the two ETGs with the largest UV upturn and high Mg2 index (Bertola et al. 1995), that have been interpreted as the signature of very metal-rich stars (Bressan, Chiosi & Fagotto 1994), have Spitzer IRS spectra similar to those observed in our passive Virgo ETGs (Bressan et al. in preparation). Thus, there seems to be no evidence that metallicity has a direct effect on mass loss.

As already anticipated, variations of age and metallicity are very well separated in this colour-colour diagram, with iso-metallicity lines being almost horizontal and coeval SSPs moving on almost vertical lines.

At an age of about 13.5 Gyr the dusty AGB phase is practically absent for any metallicity, and the models coincide with those computed without dusty AGB envelopes. Models without dusty AGB envelopes collapse to the almost horizontal dashed lines at the bottom of the diagram, independent of their ages.

We have extended the photospheric stellar spectra of MILES in the NIR/MIR region by means of matched NEXTGEN models (Hauschildt et al. 1999). In addition, the effects of dusty envelopes have been included following the prescriptions described in Bressan et al. (1998). Thus, the bottom horizontal dashed lines (models without dusty AGB envelopes) superimpose on single NEXTGEN spectra at varying effective temperature. The effect of varying the metallicity is almost negligible in the K_s -[16] colour. To illustrate the difference introduced by adopting different stellar spectra we have marked with an asterisk the position of a COMARCS low temperature atmosphere model as calculated by Aringer et al. (2008, in prep.). Finally, the hexagon towards the bottom left of the diagram (age ~ 11.5 Gyr and $Z \sim 0.005$), marks the position of the globular cluster 47 Tuc whose semi-empirical integrated colours have been derived by Bressan et al. (2006b).

Fig. 6 shows that galaxies that follow the MIR colour-magnitude relation are almost coeval, with an age of about 10 Gyr and a metallicity that grows by a factor of about two. It is interesting to note that the four Virgo galaxies are as old as the oldest Coma galaxies. None of the galaxies appear to be as old as the globular cluster 47 Tuc.

Galaxies with a K_s -[16] excess, cluster around the lines of 8 Gyr and 6 Gyr thus appearing younger by about 2-4 Gyr.

In order to clarify the different sensitivity to stellar populations of optical and MIR colours, we have reproduced, in Fig. 4, the optical/NIR colour-magnitude relation for the

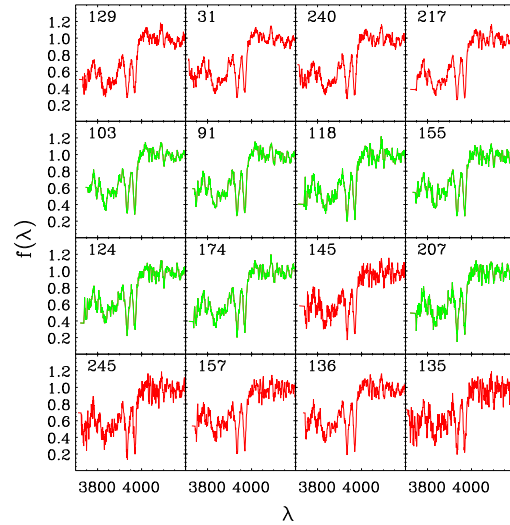


Figure 7. Optical SDSS spectra of selected Coma cluster galaxies. Galaxies with a K_s -[16] excess are shown in green.

galaxies shown in Fig. 6. Galaxies with a K_s -[16] excess (i.e. clustering around and above 8 Gyr in Fig. 6) are plotted with a cross. Fig. 4 shows that in spite of a well detected K_s -[16] excess, the latter galaxies lie on the optical/NIR colour-magnitude relation. Moreover, a significant fraction of these galaxies are classified as ellipticals.

3.3 Indirect influence of cluster environment on the K_s -[16] colour ?

The fraction of galaxies showing a K_s -[16] colour excess with respect to the oldest systems, in Fig. 6, is about 48%. If we consider the total sample (Fig. 2) and add four more galaxies with a clear K_s -[16] excess with respect to the CM relation, the fraction is about 32%.

A possible interpretation, discussed in the previous section, is that these systems have average younger ages, since a younger stellar population is expected to have a redder MIR emission by virtue of the larger fraction of dusty AGB stars. However, galaxies are complex systems that may not be well represented by simple stellar populations and caution must be used in the interpretation of the K_s -[16] colour excess. It does not necessarily point to a younger global age of a passively evolving system.

For example, in the case of the Virgo ETG, NGC 4435, Panuzzo et al (2007) have shown that the MIR emission is dominated by a nuclear starburst which is practically invisible in the optical and NIR. Its IRS low resolution spectra are dominated by PAH, atomic and molecular emission features that are typical of star forming galaxies. At $16\mu\text{m}$ the emission is not resolved, indicating that the emission arises from the nucleus; which indeed appears as a dusty disk in HST images. In this rejuvenation episode (about 200 Myr ago) less than 1% of the total galaxy mass was formed. From Panuzzo et al. (2007) we estimate, for NGC 4435, a K_s -[16] colour $\simeq 2.8$ mag in the central 5 arcsec radius aperture, and a total K_s -[16] colour $\simeq 2.1$ mag and total V-K $\simeq 3.1$. In Fig. 6, the latter values would put NGC 4435 in the region around 6 Myr and $Z=0.02$. Indeed, NGC 4435 was selected

for IRS observations as one of the galaxies that make up the Virgo colour-magnitude relation. From the analysis of this sample (18 galaxies) Bressan et al. (2006) concluded that the fraction of early-type galaxies that show signatures of recent activity is 17%. This figure is significantly lower than the fraction of Coma ETGs with a K_s -[16] colour excess.

We have also extracted, from data release 6 of the Sloan Digital Sky Survey (SDSS) the available spectra (16 out of 50) of our Coma galaxy sample. In Fig. 7 we show the 3700Å–4200Å spectral region, around the CaII lines. Galaxies are sorted by decreasing brightness and green curves represent objects with a K_s -[16] colour excess. In three objects (D103, D118 and D155) with a K_s -[16] excess, the CaII H line is as deep as the K line, indicating contamination by A type stars, i.e. a recent rejuvenation episode. In the other galaxies the CaII doublet appears normal. We recall, that for solar metallicity, an inversion of the CaII doublet starts appearing only at ages younger than 2 Gyr (Longhetti et al., 1999).

Although we see in fig. 5 that the K_s -[16] colour is uncorrelated with the position in the cluster we note that if we identify those galaxies with an ‘excess’ of 16 μ m emission as those with $K_s - [16] > 1.5$ (see fig. 2) then the mean projected distance from the cluster centre of this population is smaller than for those galaxies with $K_s - [16] < 1.5$. The mean projected distance from the cluster centre for the 16 μ m excess galaxies is 0.17° whereas that for the others is 0.32° (the KS-probability that the 2 distributions are the same is 1.6%). Because it seems that the cluster environment does not directly influence the mid-infrared colour-magnitude diagram this suggests that the star formation history has been modified by the environment; which in turn influences the galaxy colours. The sense of this influence is that galaxies with redder K_s -[16] colour (younger luminosity weighted stellar ages, fig. 6) are preferentially found at small cluster-centric radii.

Miller, Neal & Owen (2002) have investigated the distribution of both AGN and star-forming galaxies as a function of cluster-centric distance. They find that dusty star-forming galaxies have a more centrally concentrated distribution than normal star-forming galaxies, with AGN being more centrally concentrated than both. Though there is no evidence of emission lines in the SDSS spectra, we cannot exclude that the MIR excess is due to an obscured nuclear starburst like that found in NGC 4435. A possible way to check this possibility is by means of IRAC 4.5 μ m and 8 μ m observations (sampling the strength of the 7.7 PAH feature) and MIPS 24 μ m (sampling the presence of hot dust). This work is underway.

The cluster environment clearly can affect star formation; the deficit of atomic gas in late-type galaxies in clusters (e.g., Haynes, Giovanelli, & Chincarini, 1984) indeed means that these galaxies have less fuel for star formation. In the case of ETGs, the means by which the environment can influence the star formation history is less obvious, especially given that minor mergers should be less frequent in the high velocity dispersion environment of the cluster core. Transfer of angular momentum via galaxy ‘harassment’ (Moore et al. 1996) may cause infall of existing ISM and increase the probability of star formation, but if such a mechanism has been important in the last few Gyr of the cluster’s life it is not an important effect today. Observationally the star

formation rate tends to be lower toward the centre of clusters and in clusters relative to the field (Lewis et al. 2002, Gómez et al. 2003) .

3.4 Implications

The MIR colour-magnitude relation indicates that the oldest Coma early-type galaxies define a sequence of increasing metallicity at constant age ($Z \simeq 0.01 - 0.03$, $t \simeq 10.5$ Gyr).

While this conclusion has already been suggested by the analysis of the optical/NIR colour-magnitude relation, it is only with the use of the complementary MIR observations that the alternative solution (invoking a synchronization of the epoch of formation with total brightness, see Bower, Lucey & Ellis, 1992) can be excluded.

Indeed, our analysis of the mixed optical-NIR-MIR colour-colour diagram clearly shows that some of the galaxies that populate the optical colour-magnitude relation may have average ages that are even 40% younger than the old sequence. In those galaxies, however, a larger metallicity may redden the colours and compensate for the younger age in an optical diagram. This illustrates the importance of the MIR colour in breaking the age-metallicity degeneracy.

Our conclusion is in very good agreement with the analysis of narrow band indices of ~ 4000 ETGs carefully selected from the SDSS survey (Clemens et al. 2006) and recently extended to ~ 14000 objects with the DR6 catalogue (Clemens et al. 2008 in prep.). These authors find that the luminosity-weighted ages of the whole sample start low at a low velocity dispersion, increase up to a maximum at $\sigma \sim 2.32$ and then flatten above this threshold. In contrast, the metallicity shows a continuous increase with increasing σ .

Our result, that a large fraction of ETGs in Coma populate a genuine old and coeval sequence, contrasts somewhat with the recent study of ETGs in the Coma cluster by Trager et al. (2008). Based on optical spectra these authors also find that, in spite of a wide range in mass, 10/12 objects are consistent with the hypothesis of a coeval population. However, the age they find for this population, 5.2 ± 0.2 Gyr, is significantly younger than our value.

We notice that this discrepancy is unlikely to be caused by a significant offset between ages derived with the two methods. Indeed, there are four objects in common, for which Trager et al. find the following ages: D129 (GMP3329) 7.9 Gyr, D157 (GMP3484) 7.8 Gyr, D155 (GMP3367) 4.5 Gyr and D133 (GMP3639) 3 Gyr.

D129 and D157, the two old objects, fall on our MIR colour-magnitude relation, for which we derive only slightly older ages. On the other hand D155 and D133, the two young objects, lie well above this relation and, given their K_s -[16] colour we would conclude that they are possibly affected by some rejuvenation episode.

Considering that, contrary to our analysis, optical studies are affected by the age-metallicity degeneracy causing (large) uncertainties that are difficult to quantify, we believe that there is good agreement for the few objects in common.

It is more difficult to explain why we find that 68% of the galaxies in our sample populate the old sequence, while Trager et al. find that only 25% are old. If their sample is not biased toward young objects and given the sensitivity

of the K_s -[16] colour to rejuvenation events, we suspect that the age-metallicity degeneracy is still to blame.

Bregman et al. (2006) find a very similar discrepancy between the age of ETGs determined by optical line indices and mid-infrared Spitzer spectra that include the silicate emission feature near $10\ \mu\text{m}$.

They also find mean ages of ~ 10 Gyr.

It is also interesting to note that in the upper 2.5 mag the MIR colour-magnitude relation is quite narrow. On the contrary, in the lower 2.5 mag, below $M_K \sim -24.5$, there is a significant dispersion. This shows that the rejuvenation events (of any kind) do not affect the most massive ETGs.

4 CONCLUSIONS

We present 16 μm , Spitzer-IRS, blue peakup images of a sample of 50 ETGs in the Coma cluster. We compare these with archival IRAC images at 4.5 μm and 2MASS, K_s band images at 2.2 μm .

We make the following conclusions.

- Although most galaxies are unresolved at the resolution of the blue peakup array, those that are resolved have effective radii that are similar to those measured in the near-infrared by Gavazzi et al. (2000). We thus find no evidence that the 16 μm emission is either emitted by an extended inter-stellar medium or from a central point source. The mid-infrared emission is stellar in origin.

- The region within a dusty AGB star envelope where dust is hot enough to emit strongly at 16 μm is not vulnerable to environmental effects such as the ram-pressure of an ISM wind or dust sputtering by hot gas. Dust grains only spend ~ 100 yr near ~ 300 K and this region is sufficiently dense to survive against ram-pressure disruption.

- We construct the mid-infrared colour-magnitude diagram of Coma ETGs in terms of the K_s - [16] colour. We compare this with the colours of 4 ETGs in the Virgo cluster which show mid-infrared *spectra* characteristic of purely passively evolving stellar populations. In this way we identify the colour-magnitude relation of passively evolving galaxies as the lower envelope of the galaxy distribution in the K_s - [16] vs K_s plane; that is, the minimum value of K_s - [16] at a given K_s magnitude.

- We construct the mixed optical-NIR-MIR two colour diagram and, by means of updated simple stellar population models, we show that the addition of mid-infrared data allows a much better separation of the effects of age and metallicity, which are rather degenerate in either the optical or mid-infrared when taken in isolation.

- In the above two-colour diagram, galaxies populating the colour-magnitude relation trace a sequence of *varying metallicity at approximately constant age*. Although this conclusion was already consistent with the optical-NIR colour-magnitude relation, a correlation between age and metallicity could equally well explain the relation. Indeed, comparison with the optical-NIR colours shows that a *number of galaxies that lie on the optical-NIR relation are significantly displaced from the mid-infrared relation*, with redder K_s - [16] colours. The mid-infrared colour-magnitude diagram therefore shows a sequence of metallicity for old, passive galaxies, with younger objects displaced towards redder K_s - [16] colours.

- The oldest elliptical galaxies in our sample have luminosity weighted, mean stellar ages of 10.5 Gyr and metallicities within a factor of two of the solar value. No galaxy in our sample is as old or metal poor as the globular cluster 47 Tuc.

- Although the addition of the K_s - [16] colour allows us to identify objects with significantly younger, luminosity weighted, mean stellar ages, we cannot distinguish between genuinely ‘young’ objects and those that have undergone a minor rejuvenation event. However, given that even a period of recent (last few Gyr) star formation that accounts for less than 1% of the total stellar mass will shift a galaxy off the mid-infrared colour-magnitude relation, the latter option seems far more likely. Unambiguous resolution of this issue will require the infrared spectroscopic capabilities of future space observatories.

- 68% of the galaxies in our sample lie on the mid-infrared colour-magnitude relation. These galaxies cannot have had any episode of star formation accounting for more than $\sim 1\%$ of the total stellar mass within the last few Gyr. These are genuinely ‘passively evolving’ objects. This result is at odds with the most recent estimate of the fraction of old objects based on optical spectroscopy (Trager et al. 2008).

- There is evidence that those galaxies that have an excess in the K_s - [16] colour are found preferentially at smaller cluster-centric radii. As the interaction between the dusty AGB star envelopes and the ISM does not directly effect the 16 μm emission, the excess may be caused by “rejuvenation” episodes during the star formation history induced by the cluster environment.

ACKNOWLEDGMENTS

We acknowledge a financial contribution from contract ASI-INF I/016/07/0.

This work is based on observations made with the Spitzer Space Telescope, which is operated by the JPL, Caltech under a contract with NASA.

We make use of data products from the Two Micron All Sky Survey, which is a joint project of the University of Massachusetts and the Infrared Processing and Analysis Center/California Institute of Technology, funded by the National Aeronautics and Space Administration and the National Science Foundation.

This research has made use of the GOLD Mine Database.

Funding for the SDSS and SDSS-II has been provided by the Alfred P. Sloan Foundation, the Participating Institutions, the National Science Foundation, the U.S. Department of Energy, the National Aeronautics and Space Administration, the Japanese Monbukagakusho, the Max Planck Society, and the Higher Education Funding Council for England. The SDSS Web Site is <http://www.sdss.org/>.

The SDSS is managed by the Astrophysical Research Consortium for the Participating Institutions. The Participating Institutions are the American Museum of Natural History, Astrophysical Institute Potsdam, University of Basel, University of Cambridge, Case Western Reserve University, University of Chicago, Drexel University, Fermilab, the Institute for Advanced Study, the Japan Participation Group, Johns Hopkins University, the Joint Institute for

Nuclear Astrophysics, the Kavli Institute for Particle Astrophysics and Cosmology, the Korean Scientist Group, the Chinese Academy of Sciences (LAMOST), Los Alamos National Laboratory, the Max-Planck-Institute for Astronomy (MPIA), the Max-Planck-Institute for Astrophysics (MPA), New Mexico State University, Ohio State University, University of Pittsburgh, University of Portsmouth, Princeton University, the United States Naval Observatory, and the University of Washington.

We thank P. Marigo, L. Girardi and A. Renzini for useful discussions.

REFERENCES

- Annibali F., Bressan A., Rampazzo R., Zeilinger W. W., Danese L., 2007, *A&A*, 463, 455
- Aringer B. et al. 2008, *A&A* in prep.
- Athey A., Bregman J., Bregman J., Temi P., Sauvage M., 2002, *ApJ*, 571, 272
- Bernardi M., Sheth R. K., Nichol R. C., Schneider D. P., Brinkmann J., 2005, *AJ*, 129, 61
- Bertola, F., Bressan, A., Burstein, D., Buson, L. M., Chiosi, C., & di Serego Alighieri, S. 1995, *ApJ*, 438, 680
- Bower R. G., Lucey J. R., Ellis R. S., 1992, *MNRAS*, 254, 589
- Boyer, M. L., McDonald, I., van Loon, J. T., Woodward, C. E., Gehrz, R. D., Evans, A., & Dupree, A. K., 2008, *AJ*, 135, 1395
- Bregman J. N., Temi P., Bregman J. D., 2006, *ApJ*, 647, 265
- Bressan, A., Chiosi, C., & Fagotto, F., 1994, *ApJS*, 94, 63
- Bressan A., et al., 2006, *ApJ*, 639, L55
- Bressan A., Granato G.-L., Silva L., 1998, *A&A*, 332, 135
- Cappellari M., Bacon R., Bureau M., Damen M. C., Davies R. L., de Zeeuw P. T., Emsellem E., Falcon-Barroso J., Krajnovic D., Kuntschner H., McDermid R. M., Peletier R. F., Sarzi M., van den Bosch R. C. E., van de Ven G., 2006, *MNRAS*, 366, 1126
- Carraro, G., Girardi, L., Bressan, A., & Chiosi, C. 1996, *A&A*, 305, 849
- Clemens M. S., Bressan A., Nikolic B., Alexander P., Annibali F., Rampazzo R., 2006, *MNRAS*, 370, 702
- Dressler, A., 1980, *ApJS*, 42, 565
- Dwek E., Rephaeli Y., Mather J.C., 1990, *ApJ*, 350, 104
- Gavazzi G., Franzetti P., Scodreggio M., Boselli A., Pierini D., 2000, *A&A*, 361, 863
- Gavazzi G., Boselli A., Donati A., Franzetti P., Scodreggio M., 2003, *A&A*, 400, 451
- Gledhill T. M., Yates J. A., 2003, *MNRAS*, 343, 880
- Gómez P. L., et al., 2003, *ApJ*, 584, 210
- Hauschildt, P. H., Allard, F., Ferguson, J., Baron, E., & Alexander, D. R., 1999, *ApJ*, 525, 871
- Haynes M. P., Giovanelli R., Chincarini G. L., 1984, *ARA&A*, 22, 445
- Landsman W.B., 1995, *ASP Conference Series*, 77, 437
- Lebzelter, T., Posch, T., Hinkle, K., Wood, P. R., & Bouwman, J. 2006, *ApJ*, 653, L145
- Leeuw L. L., Sansom A. E., Robson E. I., Haas M., Kuno N., 2004, *ApJ*, 612, 837
- Lewis I., et al., 2002, *MNRAS*, 334, 673
- Longhetti, M., Bressan, A., Chiosi, C., & Rampazzo, R., 1999, *A&A*, 345, 419
- Marleau F. R., et al., 2006, *ApJ*, 646, 929
- Miller, Neal A.; Owen, Frazer N., 2002, *AJ*, 124, 2453
- Moore B., Katz N., Lake G., Dressler A., Oemler A., 1996, *Nature*, 379, 613
- Origlia, L., Rood, R. T., Fabbri, S., Ferraro, F. R., Fusi Pecci, F., & Rich, R. M., 2007, *ApJ*, 667, L85
- Panuzzo P., et al., 2007, *ApJ*, 656, 206
- Renzini, A., 2006, *ARA&A*, 44, 141
- Sánchez-Blázquez P., Gorgas J., Cardiel N., González J. J., 2006b, *A&A*, 457, 809
- Sánchez-Blázquez P., et al., 2006b, *MNRAS*, 371, 703
- Temi P., Brighenti F., Mathews W. G., 2008, *ApJ*, 672, 244
- Temi P., Brighenti F., Mathews W. G., 2007, *ApJ*, 660, 1215
- Thomas D., Maraston C., Bender R., Mendes de Oliveira C., 2005, *ApJ*, 621, 673
- Trager S. C., Faber S. M., Dressler A., 2008, *MNRAS*, 386, 715
- van Loon, J. T., Boyer, M. L., & McDonald, I., 2008, *ApJ*, 680, L49
- Young P. J., 1976, *AJ*, 81, 807

APPENDIX A: IRS BLUE PEAKUP IMAGES

This paper has been typeset from a \LaTeX file prepared by the author.

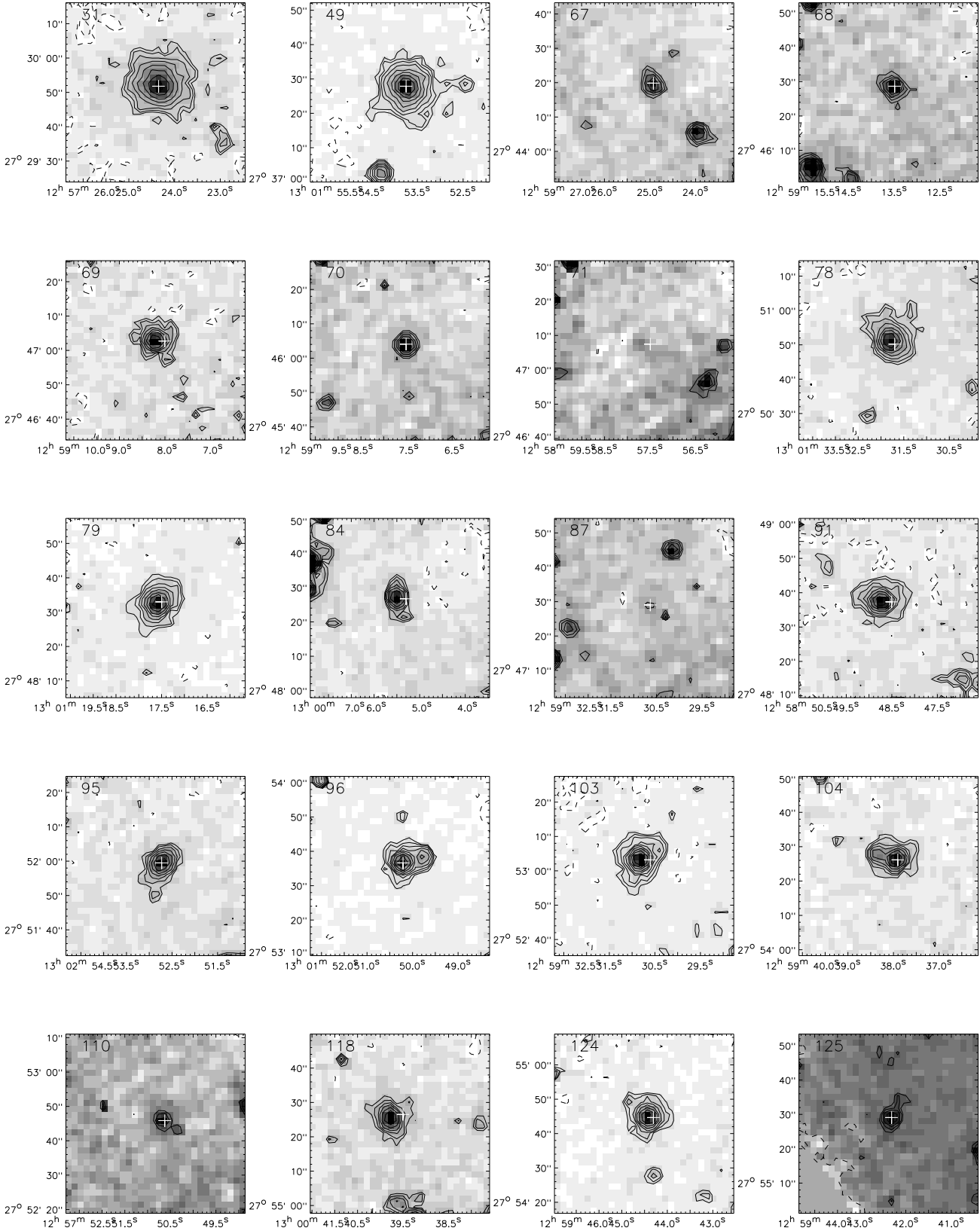


Figure A1. Background subtracted, PBCD, IRS peakup images of the Coma ETGs. Contour levels are $2^{n/2}/100$ where $n=(-1,0,1,2,\dots)$ mJy/pixel with a dashed contour for negative values at the lowest level. The grey-scale in each plot is scaled to the peak source flux. The last panel is an image of the peak-up point spread function. The cross in each panel gives the optical source position. The grey-scale has a square-root stretch and contour levels are $2^{n/2}/100$ where $n=(1,3,5,\dots)$ mJy/pixel. Pixels are $1''.8$ on a side.

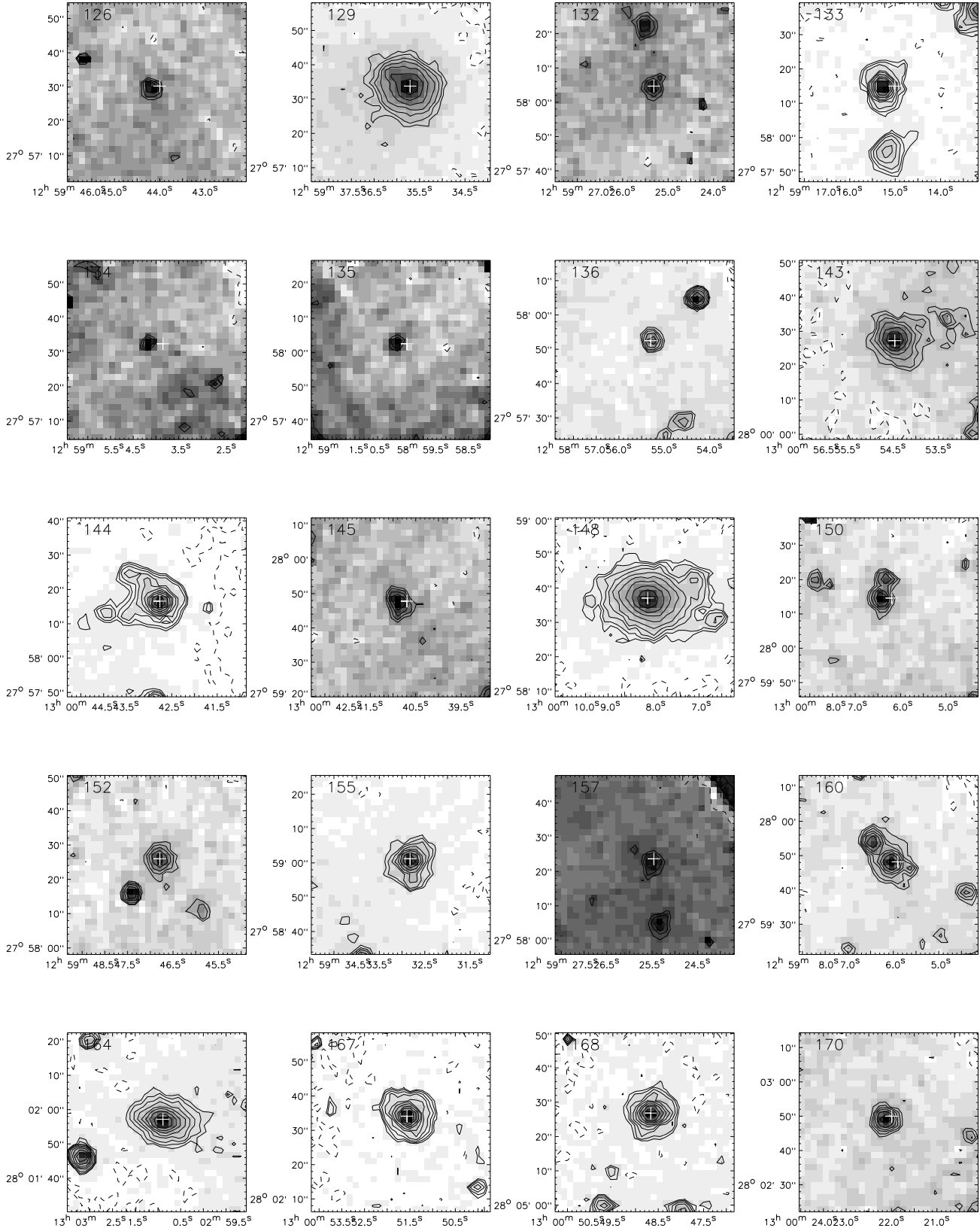


Figure A1. Cont.d

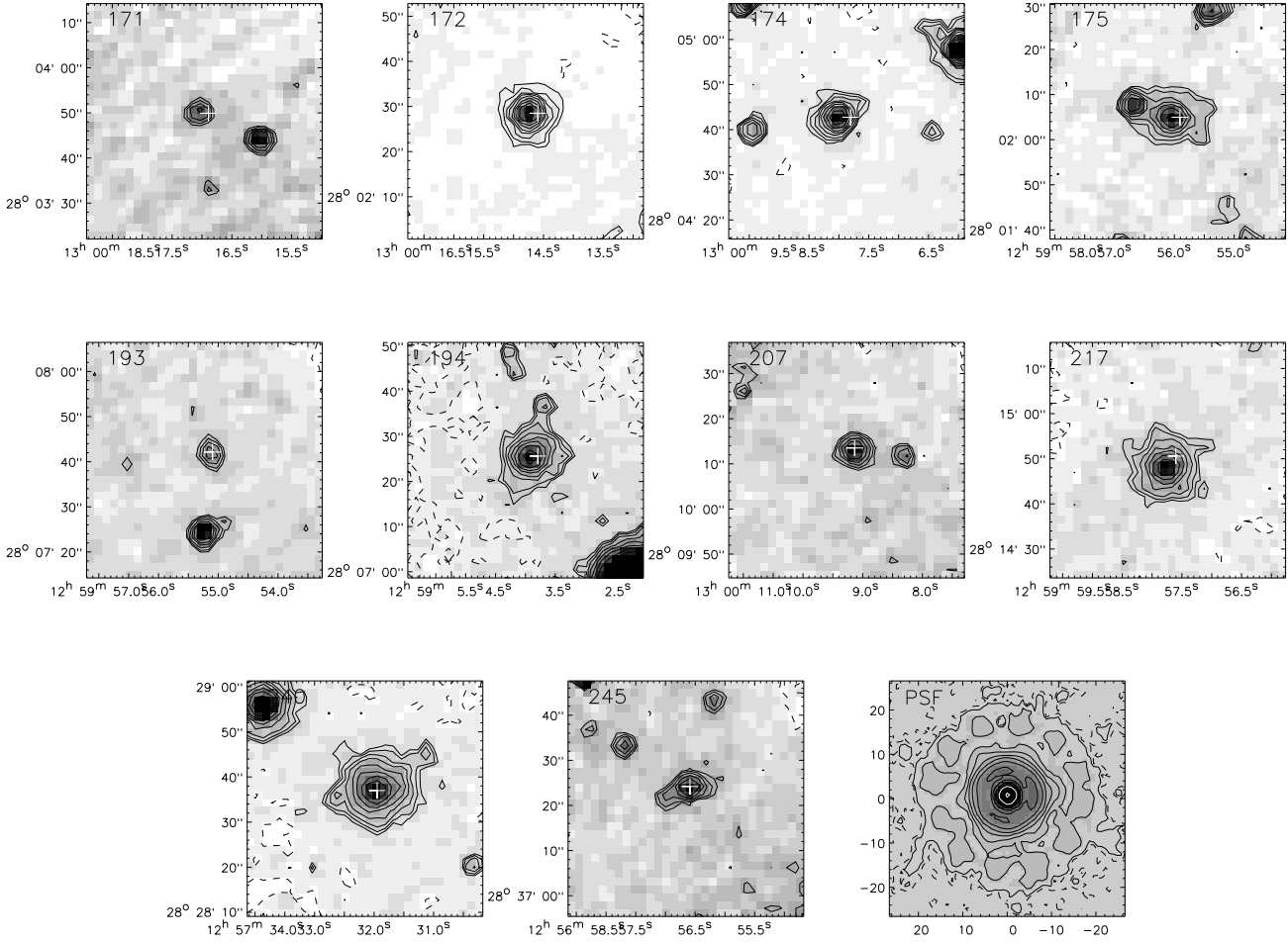


Figure A1. Cont.d